Radiation Pressure Acceleration by X-rays in Active Galactic Nuclei

Doron Chelouche* and Hagai Netzer*

School of Physics and Astronomy and the Wise Observatory, The Beverly and Raymond Sackler Faculty of Exact Sciences,
Tel Aviv University, Tel Aviv 69978, Israel

1 February 2008

ABSTRACT
We present calculations of the dynamics of highly ionized gas clouds that are confined by external pressure, and are ionized by AGN continuum. We focus on the gas that is seen in absorption in the X-ray spectrum of many AGN and show that such gas can reach hydrostatic equilibrium under various conditions. The principal conclusion is that the clouds can be accelerated to high velocities by the central X-ray source. The dynamical problem can be reduced to the calculation of a single parameter, the average force multiplier, $\langle M \rangle$. The typical value of $\langle M \rangle$ is ~ 10 suggesting that radiation pressure acceleration by X-rays is efficient for $L/L_{\rm Eddington} \gtrsim 0.1$. The terminal velocity scales with the escape velocity at the base of the flow and can exceed it by a large factor. The typical velocity for a HIG flow that originates at $R = 10^{17}$ cm in a source with $L_x = 10^{44}$ erg s^{-1} is ~ 1000 km s^{-1}, i.e. similar to the velocities observed in several X-ray and UV absorption systems.

Highly ionized AGN clouds are driven mainly by bound-free absorption and bound-bound processes are less important unless the lines are significantly broadened or the column density is very small. Pressure laws that result in constant or outward decreasing ionization parameters are most effective in accelerating the flow.

Key words: ISM: jets and outflows — galaxies: active — galaxies: nuclei — quasars: absorption lines — X-rays: general

1 INTRODUCTION

Highly ionized gas (HIG) is common in both types of active galactic nuclei (AGN). It is seen as strong absorption features in many type-I (Seyfert 1) galaxies (Reynolds 1997; George et al. 1998, Kaspi et al. 2000 and references therein) and as strong, large equivalent width emission lines in many type-II (Seyfert 2) AGN (e.g. Turner et al. 1997; Netzer, Turner & George 1998). The situation regarding the high luminosity AGN (the bright quasars, see George et al. 2000 for review and references) is still unclear, mostly because of the limited signal-to-noise ASCA observations used in such studies.

The strongest observed HIG features in type-I AGN are several absorption edges, at around 1 keV, mostly due to O VII (0.74keV) & O VIII (0.87keV). The deduced hydrogen column density is in the range of $10^{21} - 10^{24}$ cm^{-2}, the covering fraction is close to unity and the ionization parameter about two orders of magnitude larger than the broad line region (BLR) ionization parameter (George et al. 1998).

Recent *Chandra* observations reveal the presence of numerous absorption and emission lines (e.g., Kaspi et al. 2000). The absorption lines are narrow (~ 150 km s^{-1})and exhibit outflow velocities of $\lesssim 1000$ km s^{-1}. Currently, there is no clear indication regarding the location and hence the mass of this component. The very few observations of variable absorption features (e.g., Guainazzi et al. 1996; and references therein) suggest a dimension not too different from that of the BLR. If correct, this would mean that the HIG observed in type-II AGN is of different origin since its distance from the centre must be larger than ~ 10 pc.

Many type-I AGN show also narrow UV absorption features due to C IVλ1548 and other resonance lines. In most cases the lines are blueshifted with respect to the systemic velocity, implying outflow with typical velocities of ~ 1000 km s^{-1}. In several well studied cases the lines are resolved, showing intrinsic width of $100 - 300$ km s^{-1} (Crenshaw et al. 1999; Crenshaw & Kraemer 1999; Srianand 2000; and references therein). There have been several suggestions linking the origin and dynamics of the UV and X-ray absorption features (Mathur et al. 1994; Mathur et al. 1995; Murray & Chiang 1995). This issue is still under discussion

---

* email: doron@wise.tau.ac.il; netzer@wise.tau.ac.il

(e.g. the new observations of 3C288.1 by Hamann, Netzer & Shields 2000).

Radiation pressure driven flows are thought to be common in astrophysical environments. Stellar winds can be accelerated to their observed velocities ($\gtrsim 1000$ km s^{-1}) by radiation pressure force (e.g., Castor, Abbott & Klein 1975). Broad absorption line (BAL) flows in AGN (BALQSO) can be driven to sub-relativistic velocities ($\sim 30,000$ km s^{-1}) by the same physical mechanism (e.g., Arav, Li & Begelman 1994; Murray et al. 1995; Proga, Stone & Kallman 2000) although other mechanisms have also been proposed (Begelman, de Kool & Sikora 1991). In both cases, the absorption line widths are of the order of the outflow velocity which lead to a continuous flow geometry. In this case, the physics can be described by the Sobolev approximation which is valid provided the velocity changes on length scales over which the other gas properties (e.g., ionization state, temperature, density) do not change considerably. Obviously not all types of flow can be driven by radiation pressure forces, among these are jets and supernovae envelopes.

A second, almost orthogonal approach to the study of flows is to consider moving "clouds" or condensations (hereafter, the "cloud model"). Such clouds are confined by means of external pressure and are likely to be in hydrostatic equilibrium. These models have been studied thoroughly in the context of broad line region (BLR) dynamics (e.g., Blumenthal & Mathews 1979; Mathews 1986). The clouds are assumed to be accelerated ballistically, with no appreciable inner velocity gradients and their spectra consists of narrow, blueshifted absorption lines (e.g., Mathews 1975). Cloud confinement and stability have been studied, extensively, in many works (e.g., Krolik 1979; Mathews 1986; Mathews 1992). Possible confinement mechanisms include thermal confinement (e.g., Krolik, McKee & Tarter 1981) with its well known problems (e.g., Mathews & Ferland 1987), and nonthermal confinement, e.g., by magnetic fields (Rees 1987; Bottorff, Korista & Shlosman 2000). Despite the many unresolved issues, the cloud model has had great success in accounting for the observed features of the BLR clouds (e.g. Netzer 1990), NLR clouds (e.g., Kraemer, Ruiz & Crenshaw 1998), and BAL flows (e.g. Arav et al. 1994).

While acceleration by UV radiation, in AGN, has been studied extensively, there are only very few works discussing the acceleration by X-ray radiation (e.g., Mathews & Capriotti 1985; Mathews & Veilleux 1989, none in great detail). In particular, there is no systematic study of the acceleration of gas with properties similar to those commonly observed in the X-ray spectrum of many AGN (for a heuristic treatment of the problem see Reynolds & Fabian 1995, for a magneto-hydrodynamical model with comparison to observations see Bottorff, Korista & Shlosman 2000). As shown below, considerations of the relevant parameter space within the framework of the cloud model, result in very different dynamics for the HIG clouds compared with previous works.

This paper investigates the acceleration of the HIG clouds. The purpose is to study the micro-physics of the gas and the radiation pressure force, and to derive the gas velocity under various conditions prevailing in type I AGN. This will enable to explain observed spectral features in new, high resolution X-ray spectra.

The paper is organized as follows: in §2 we outline the main ingredients of the model. Section 3 describes the cal-culation procedure, and present the results concerning the cloud structure, the radiation pressure force and the gas motion, with a following discussion on the model limitations. The main conclusions are summarized in §4.

2   THE MODEL

2.1   Basic assumptions

Our purpose is to solve for the structure and the dynamics of HIG clouds in AGN. Such gas has been detected by ASCA and earlier missions but the evidence used here is found mainly in the recent *Chandra* observations such as the one reported in Kaspi et al. (2000) for NGC 3783 and in Kaastra et al (2000) for NGC 5548. In both cases there is a rich absorption spectrum indicating high level of ionization, large column density ($\sim 10^{22}$ cm^{-2}) and outflow motion of $\lesssim 1000$ km s^{-1}. The lines are barely resolved (Kaspi et al. 2001) and the typical Doppler width is (~ 300 km s^{-1}). The observed properties are, therefore, different from those found in stellar winds and in BAL quasars. They can be interpreted as either due to cloud motion or continuous wind. This paper addresses the first possibility and the wind solution will be discussed in a future publication.

The main assumptions regarding the cloud model are (see also §3.5):

(i) The general AGN environment can support various type of clouds. Known examples are the BLR and the NLR clouds (e.g. Netzer 1990; see a recent study by Kaiser et al. 2000). Such entities with higher level of ionization cannot be ruled out by any known AGN property and have, in fact, been addressed, by several recent publications (e.g., Contini & Viegas 1999; Bottorff et al. 2000). The HIG region is modeled as a spherical cloud system of large covering factor. The justification is that such regions are very common in low luminosity AGN (e.g. George et al. 1998). We concentrate on thin spherical shells although this is not a requirement of the model (see §3.5.)

(ii) We assume that the clouds are confined by external pressure P_{ext}. This is required since clouds which are not self-gravitating evaporate on sound crossing time scales (which is typically much shorter than dynamical time scales). While the origin of this pressure is not the topic of the paper, we note that confinement by a hot gas (e.g. Krolik, McKee & Tarter 1981) is problematic (Mathews & Ferland 1987) and magnetic pressure is the most likely explanation (see Rees (1987) for a general formulation, de Kool & Begelman (1995) for a discussion of radiatively driven, magnetically confined flows and Sivron & Tsuruta (1993) for a discussion of the magnetically confined cloud model). The pressure is assumed to be time-independent and its radial dependence is given by

$$P_{\text{ext}} \propto R^{\alpha}, \tag{1}$$

Typically, $-10/3 \leq \alpha \leq -3/2$ (e.g., Netzer 1990). The global spherical symmetry is not critical to our discussion and is relaxed in §3.5.

(iii) We restrict the discussion to geometrically thin HIG clouds, $\Delta R/R \ll 1$ where R is the location of the *illuminated surface* (see for example Reynolds & Fabian 1995). This is based on variability studies which set rough lower limits on

the density ($\sim 10^6$ cm^{-3}, see Otani et al. 1996; Guainazzi et al. 1996) and thus, through the known ionization parameter (see below) on the location of the clouds. The external pressure difference $\Delta P_{\rm ext} \equiv P_{\rm ext}(R) - P_{\rm ext}(R + \Delta R)$ satisfies $\Delta P_{\rm ext}/P_{\rm ext} = -\alpha \Delta R/R \ll 1$. This assumption is checked for self-consistency in §3.5.

(iv) The clouds are assumed to be in photo-ionization equilibrium. This is justified as long as the recombination time is the shortest time scale. This is true in our parameter range provided the ionizing continuum is not rapidly varying (Krolik & Kriss 1995).

(v) The dynamical problem is treated by assuming radiation pressure force, gas pressure force, and gravity. The local gas acceleration, $a(r)$, at position r inside a cloud whose illuminated face is at a distance R from the centre, is given by

$$a(r) = a_{\rm rad}(r) - g - \frac{1}{\rho}\frac{dP_{\rm gas}}{dr} \qquad (2)$$

where $a_{\rm rad}$ is radiation pressure acceleration pressure, g the gravitational acceleration, ρ the gas density, and $P_{\rm gas}$ the gas pressure. Note that the dependence of g and $a_{\rm rad}$ on R has been omitted since R is constant across the geometrically thin cloud. Furthermore, we assume quasi-hydrostatic cloud structure in the cloud's rest frame. As shown by Blumenthal & Mathews (1979), and others, this is an adequate description of BLR and similar clouds. The clouds considered here are illuminated by the same radiation field and are roughly at the same location, hence the same general arguments apply. The clouds are therefore regarded as moving with a certain, distance dependent, bulk velocity and acceleration ($\langle a \rangle$, i.e., $a(r) = \langle a \rangle$), with no significant velocity gradients. Given this, we do not have to treat the full hydrodynamic problem but assume that the clouds remain stable and do not disperse as they are accelerated. The quasi-hydrostatic assumption is checked for self-consistency in §3.5.

2.2 Ionization structure and radiation pressure force

The ionization structure of the cloud is determined by the local radiation field. This is usually described in terms of the illuminated face ($r = 0$) ionization parameter, U,

$$U = \frac{\int_{\nu_0}^{\nu_1} (L_\nu/h\nu)\,d\nu}{4\pi R^2 n_H c} \qquad (3)$$

where L_ν is the monochromatic continuum luminosity (erg s^{-1} Hz^{-1}), n_H the hydrogen number density at $r = 0$ and c the speed of light. Our aim is to study the acceleration of highly ionized clouds. We therefore use the X-ray ionization parameter, U_x (Netzer 1996), defined by $h\nu_0 = 0.1$ keV and $h\nu_1 = 10$ keV. The ionization and thermal structure are calculated by ION99, the 1999 version of the photo-ionization code ION (Netzer 1996, and references therein). The code is very detailed regarding X-ray related processes and solves for the temperature profile and the radiation pressure force distribution inside the cloud. All our calculations apply to fully exposed clouds (i.e., no obscuration or shielding).

The absorption of continuum radiation by bound-bound, bound-free, Compton scattering and free-free processes results in a net momentum transfer to the clouds. The relative importance of the various processes depends
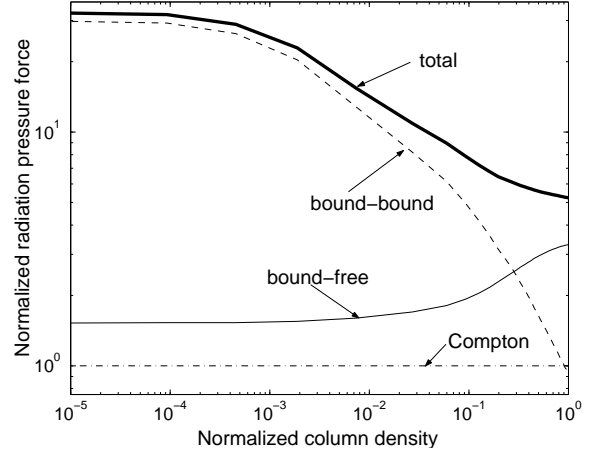

Figure 1. Contribution of various radiative processes to the normalized radiation pressure force (relative to the Compton radiation pressure force) for the standard case with line width given by $v_{\rm sound}$. Note the sharp decline of the bound-bound contribution, after $\sim 1\%$ of the total column, due to optical depth in the lines.

on the atomic cross sections and the spectral energy distribution (SED). The largest cross sections are for bound-bound transitions. These occur at energies lower than the ionization energy of the relevant ion where, for the assumed AGN-type SED (see below) the value of L_ν is larger than its value at the ionization threshold. However, large cross sections imply large optical depths and self shielding. Thus, bound-bound absorption contributes the most at the illuminated surface and decays quickly into the cloud (Fig. 1). Bound-free processes are the next largest contributers. The Compton cross-section is relatively small, and the optical depth is negligible in all cases considered here (column density $< 1.5 \times 10^{24}$ cm^{-2}). Thus, Compton scattering contributes equally (per particle) across the cloud. In almost all cases (see however §3.1), free-free absorption contributes very little to the radiation pressure force (~ 0.01 Compton). We neglect internal line radiation pressure (see Elitzur & Ferland 1986) which do not contribute significantly to the total pressure because of the low excitation temperature of the strongest X-ray transitions.

We use the force multiplier formalism (e.g., Mihalas & Mihalas 1999). The force multiplier is defined as the ratio between the radiation pressure force due to all processes relative to the force due to Compton scattering,

$$M(r) \equiv \frac{\int_0^\infty \chi_\nu(r) L_\nu e^{-\tau_\nu(r)}\,d\nu}{n_e(r)\sigma_T L_{\rm tot}}, \qquad (4)$$

where $\chi_\nu(r)$ is the frequency dependent total absorption and scattering coefficient, n_e is the number density of free electrons, $L_{\rm tot}$ is the total, unattenuated ($r = 0$) luminosity, and $\tau_\nu(r)$ is the position dependent optical depth. This gives

$$a_{\rm rad}(r) = \frac{n_e(r)\sigma_T L_{\rm tot}}{4\pi R^2 \rho(r) c} M(r). \qquad (5)$$

2.3 Model parameters

Several parameters influence the solution. The SED determines the ionization structure and the radiation pressure

force over the various energy bands. We have experimented with several SEDs typical of type-I AGN and found only little differences regarding the structure and dynamics of the clouds. We therefore take as our standard and only case an SED characterized by a "UV bump", $\alpha_{ox} = 1.4$, $\alpha_{(0.5-1\ keV)} = 1.06$, and $\alpha_{(1-10\ keV)} = 0.9$.

The internal line widths determine the line optical depth and thus the bound-bound contributions to $\langle M \rangle$. We have experimented with three possibilities: a) Thermal line width, v_T. b) Gaussian-shaped profiles with line widths for all ions equal to the thermal hydrogen line width (denoted by $v_{\rm sound}$). c) Gaussian-shaped, line profiles, characterized by their FWHM (typically several hundred km s^{-1}) and motivated by the Crenshaw et al. (1999) and Kaspi et al. (2001) observations. Mechanisms responsible for such broadening have been discussed, extensively, in the literature (see Bottorff & Ferland (2000) for discussion of MHD turbulences, including many older references, as well as many papers discussing microturbulences and expansion in stellar atmospheres).

The range of ionization parameter and column density is determined by the observations (Reynolds & Fabian 1995; Reynolds 1997; George et al. 1998; Kaspi et al. 2001). We chose $0.02 < U_x < 4$ and $10^{20} \leq N_H \leq 10^{23}$ cm^{-2}. Many of the results pertain to a "standard model" defined by $U_x = 10^{-0.8}$, $n_H = 10^8$ cm^{-3}, $N_H = 10^{22}$ cm^{-2}, with line width given by v_T. We consider only the following solar-like composition, H : He : C : N : O : Ne : Mg : Si : S : Ar : Fe = $10^4 : 10^3 : 3.7 : 1.1 : 8 : 1.1 : 0.35 : 0.37 : 0.16 : 0.03 : 0.4$

2.4   Method of solution

We follow the general method described in Weymann (1976), Mathews & Blumenthal (1977) and Blumenthal & Mathews (1979) where the cloud structure obeys the hydrostatic equation

$$\frac{dP_{\rm gas}(r)}{dr} = \rho(r)\left[a_{\rm rad}(r) - g - \langle a \rangle\right], \qquad (6)$$

where $\langle a \rangle$ is the average (bulk) acceleration. This is satisfied for every distance R. The radiation pressure force is changing across the cloud due to optical depth effects. This results in a non-uniform gas pressure profile which must obey the boundary condition $P_{\rm gas}(r = 0) = P_{\rm ext}(R) \approx P_{\rm ext}(R + \Delta R) = P_{\rm gas}(r = \Delta R)$. The exact distribution depends on the ionization structure, the level population of the various ions, and the temperature at every point inside the cloud.

The cloud accelerates ballistically and we make no use of the continuity equation. Nevertheless, the cloud column density can change due to the external conditions since it can accrete mass, lose mass, or expand along the way. In this work we treat the 1D problem and consider the following $N_H(R)$: 1) constant mass gas shells which subtend a constant solid angle, $\Omega \leq 4\pi$, i.e. $\Omega R^2 N_H = $ const, 2) constant column density clouds. The latter model is included as an example for extreme cases where the column density decreases with distance much slower than R^{-2}. For example, spherical constant mass clouds imply $N_H \propto R^{2/3\alpha}$. This allows us to study the sensitivity of our results to different column densities. In §3.5 we consider several other implications of these assumptions.

To calculate the acceleration $\langle a \rangle$, we integrate equation (6) with the given boundary conditions (i.e., pressure) at both cloud surfaces. Given our parameter space and set of assumptions, the contribution of the small external pressure gradients to the acceleration via $\Delta P_{\rm ext}/(\rho \Delta R)$ is negligible ($\sim 10^{-4}g$) and the bulk acceleration is given by

$$\langle a \rangle = \frac{\int_0^{\Delta R} \rho(r)a_{\rm rad}(r)dr}{\int_0^{\Delta R} \rho(r)dr} - g, \qquad (7)$$

which depends on R via the boundary conditions, the value of N_H and via $a_{\rm rad}(r)$.

Keeping with the definition of the average acceleration, we define the average force multiplier,

$$\langle M \rangle = \frac{\int_0^{\Delta R} n_e(r)M(r)dr}{\int_0^{\Delta R} n_e(r)dr}, \qquad (8)$$

where we have made use of the fact that U_x is large and hydrogen and helium are fully ionized, thus $\rho(r)/n_e(r) \sim 1.18 m_H$. Thus we obtain the hydrostatic equation in the force multiplier representation,

$$\frac{dP_{\rm gas}(r)}{dr} = \frac{n_e(r)\sigma_T L_{\rm tot}}{4\pi R^2 c}\left[M(r) - \langle M \rangle\right]. \qquad (9)$$

The cloud dynamics is therefore reduced to the ballistic case where the cloud is accelerated coherently with the following equation of motion

$$v\frac{dv}{dR} = \langle a(R) \rangle = \frac{1}{1.18 m_H}\frac{\sigma_T L_{\rm tot}}{4\pi c R^2}\langle M(R) \rangle - \frac{GM_{\rm BH}}{R^2} \qquad (10)$$

where v is the velocity of the cloud and $M_{\rm BH}$ is the mass of the central black hole. Thus, $\langle M \rangle$ is the only parameter which depends on the inner structure of the cloud.

Defining a new variable, l, which is proportional to $1/M_{\rm BH}$, by

$$l = \frac{1}{1.18 m_H}\frac{\sigma_T L_{\rm tot}/c}{4\pi GM_{\rm BH}} = \frac{L_{\rm tot}}{1.18 L_{\rm edd}}, \qquad (11)$$

simplifies the equation of motion to

$$v\frac{dv}{dR} = \frac{1}{1.18 m_H}\frac{\sigma_T L_{\rm tot}}{4\pi c R^2}\left(\langle M(R) \rangle - \frac{1}{l}\right). \qquad (12)$$

In the above formalism, the dynamical problem is decoupled from the cloud structure problem (i.e. the structure is independent of the cloud velocity).

The actual calculations start by assuming a uniform density profile and by solving for the temperature and radiation pressure force profiles. We calculate $\langle M \rangle$, solve the hydrostatic equation and obtain the first estimate of $P_{\rm gas}(r)$. Given the first temperature profile, we obtain a new density profile which is used, as an input, for the next iteration. This procedure is repeated several times until convergence. Tests show that the final results depend very little on the initial density profile. The iteration stops when the density profile does not change by more than 1% between one iteration to the next.

Given the pressure and ionization profile, the solution of the equation of motion is straight forward. The initial conditions include the distance from the centre at the base of the flow, R_0, $P_{\rm ext}(R_0)$, $N_H(R_0)$, the column density as a function of R (i.e., constant column clouds or constant mass shells), and the AGN parameters (α, $L_{\rm tot}$ and l). This allows us to solve for the cloud structure and for $v(R)$ at each R.

3   RESULTS AND DISCUSSION

This section describes the results of the calculations regarding the cloud's internal structure, the average force multiplier $\langle M \rangle$, and the cloud motion. Unless otherwise specified the standard model parameters are assumed.

3.1   Cloud structure

We allow the ionization parameter to vary in the range $10^{-1.8} - 10^{0.6}$ assuming all other parameters remain constant. The contributions of the various absorption and scattering processes to M are computed from the ionization structure. As seen in Fig. 2, the force multiplier decreases with U_x. The reasons are the fewer bound-bound transitions at large U_x and the lower available driving flux at high energies.

A common property of all models is the increasing density into the cloud (Fig. 2), due to the temperature decrease as a function of r and the constant external pressure. The most extreme case shown here is for $U_x = 10^{-0.8}$ where the density increases by a factor ~ 2 above its initial value. This is also the ionization parameter where the ionization and thermal structure are dominated by H-like and He-like oxygen.

Fig. 2 also shows the internal pressure profile. The rise near $r = 0$ is caused by the pressure gradient that must balance the radiation pressure force which is larger at this location due to the contribution of bound-bound processes. The peak pressure depends on the difference $M(r = 0) - \langle M \rangle$ and the location r where $M(r) = \langle M \rangle$. For very large values of U_x, the peak is lower since the gas is highly ionized and bound-bound transitions are less important.

Finally, since the value of the temperature at the illuminated surface, T, is independent of the column density, we can approximate it by $T \simeq 10^{5.5} U_x^{0.5}$ which is a good approximation for the abundances, SED and the range of U_x considered here. The same functional form, with different coefficients, provides a good fit for other SEDs (see, e.g., Komossa & Meerschweinchen 2000).

Changes in column density affect the pressure and temperature profile because of the increased opacity. This is shown in Fig. 3. For low column densities, and the standard U_x, the clouds have almost uniform ionization structure. The ionization structure and the radiation pressure force distribution change considerably for $N_H \geq 10^{22}$ cm^{-2} since this column density corresponds to an optical depth of ~ 1 in the O VII and O VIII bound-free transitions.

A common feature for all column densities is the fast decline of the bound-bound force multiplier, M_{bb}, beyond $N_H \geq 10^{17}$cm^{-2}, due to the large line opacity. Deeper layers contribute much more to the bound-free force multiplier, M_{bf}. This behavior is column density dependent since, for large columns, the increased bound-free opacity causes lower energy bands of the continuum to become more significant in producing the local radiation pressure (for the typical SED considered here, there are many more photons in these bands). The increase in M_{bf} is the reason for the peculiar pressure profile in the $N_H > 10^{22}$ cm^{-2} models.

We study clouds with a large range of densities ($1 < n_H < 10^{14}$ cm^{-3}) at the illuminated surface. As shown in Fig. 4, the cloud structure is not very sensitive to n_H for
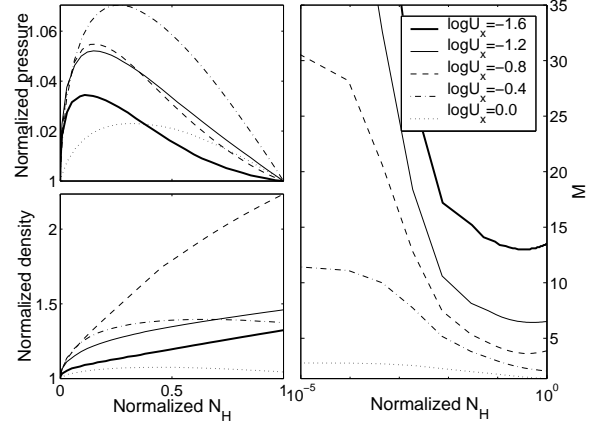

Figure 2. Density, pressure and force multiplier across the cloud for various values of U_x. In all cases $N_H = 10^{22}$ cm^{-2} and the lines have thermal profiles. The most pronounced difference is in $M(r)$, where for lower U_x, bound-bound processes contribute more near the illuminated surface with a sharper decline towards the outer surface.
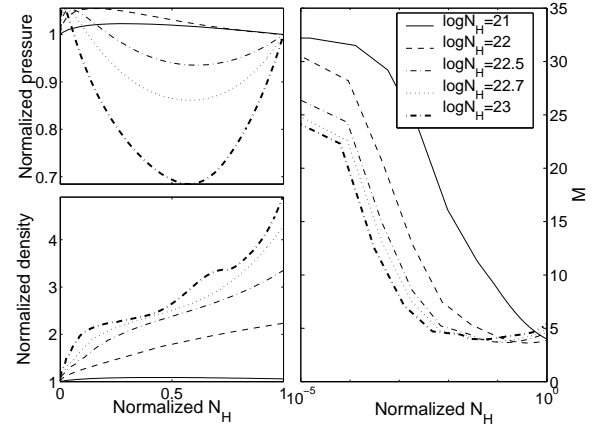

Figure 3. Cloud structure for various N_H. The cloud becomes highly non-uniform with increasing N_H and the radiation pressure force rises towards the leading, non-illuminated edge (see the $N_H = 10^{23}$ cm^{-2} curve)

.

$n_H(r = 0) \leq 10^{11}$ cm^{-3} since the micro-physics remains essentially unchanged. All changes can therefore be reduced to a scale change in ΔR. Above $n_H = 10^{11}$ cm^{-3}, the micro-physics changes considerably due to collisional excitation and free-free heating. This results in more uniform temperature and density profiles and hence changes in M_{bb}. In general, the very high density clouds are characterized by higher ionization, higher temperature and smaller M.

The internal velocity spread is dynamically important. Wider profiles decrease the line opacity and increase the thickness of the zone where $M(r)$ is dominated by bound-bound transitions. This shifts the peak of the pressure profile deeper into the cloud (Fig. 5). A large FWHM does little to affect the local ionization and temperature balance, as expected from purely radiative considerations. However, the increased importance of M_{bb} results, in low column density clouds, in a more uniform pressure profile.
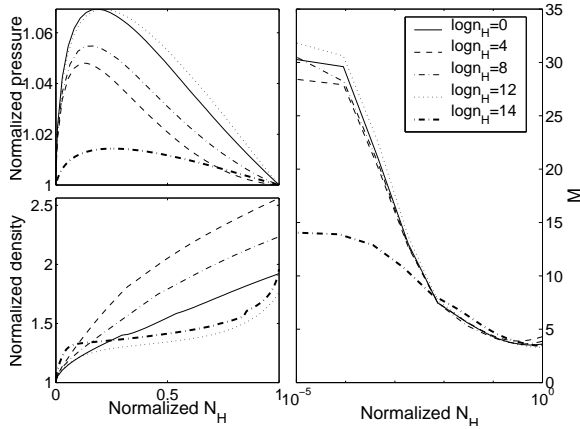
Figure 4. Density and pressure profiles for different values of $n_H(r = 0)$. The shape of the density profile is similar in all cases up to $n_H \simeq 10^{12}$ cm^{-3}, beyond which the micro-physics change considerably (see the $n_H = 10^{14}$ cm^{-3} case on the right-hand side).
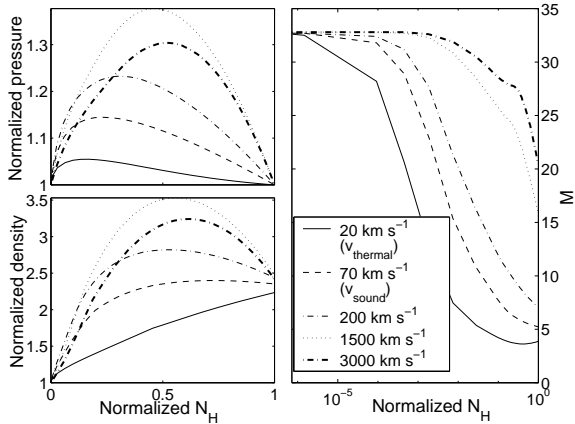

Figure 5. Cloud structure for several FWHM values of oxygen lines. The monotonic change in density, pressure, and $M(r)$ is the result of the increasing importance of bound-bound transitions. Note that for FWHM=3000 km s^{-1}, the bound-bound processes contribute significantly to $M(r)$ even at the leading (non-illuminated) surface.

3.2 The dependence of $\langle M \rangle$ on U_x, N_H, n_H and the line width

The average force multiplier is the primary property determining the cloud velocity. It is therefore important to investigate its behavior as a function of the cloud properties.

The dependence of $\langle M \rangle$ on the ionization parameter, U_x is shown in Fig. 6. Since the clouds are more ionized for larger U_x, $\langle M \rangle$ is more sensitive to higher frequency bands, where the incident flux is lower. The result is that $\langle M \rangle$ is a decreasing function of U_x for all column densities. For low column densities ($N_H < 10^{22}$ cm^{-2}) the change in $\langle M \rangle$ is roughly linear with U_x. For larger columns, the structure is more complicated (e.g., Fig. 3) and so is the dependence on U_x. A crude approximation of the form $\log \langle M(U_x) \rangle = C_1 + C_2 \log(U_x)$, for several column densities and for line widths given by v_{sound}, is
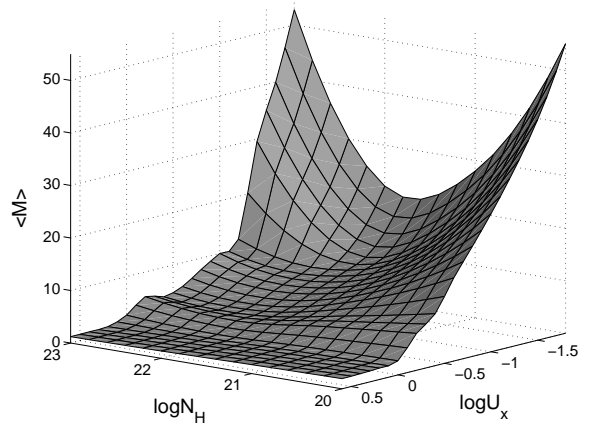

Figure 6. $\langle M \rangle$ as a function of the ionization parameter, U_x, and the column density, N_H. A monotonic decline of $\langle M \rangle$ with U_x is evident for all N_H. For $U_x > 10^{0.5}$, the cloud is highly ionized and Compton scattering dominates the radiation pressure force. $\langle M \rangle$ obtains a minimum as a function of N_H for $N_H \sim 10^{22}$ cm^{-2} for $U_x < 1$. The increase in $\langle M \rangle$, for $N_H > 10^{22}$ cm^{-2}, is the result of the changing ionization balance (see text).

$$
\log \begin{pmatrix} \langle M \rangle_{20} \\ \langle M \rangle_{21} \\ \langle M \rangle_{22} \\ \langle M \rangle_{23} \end{pmatrix} = \begin{pmatrix} -0.7 \\ -0.6 \\ -0.5 \\ -0.7 \end{pmatrix} \log(U_x) + \begin{pmatrix} 0.6 \\ 0.5 \\ 0.4 \\ 0.4 \end{pmatrix}, \quad (13)
$$

where $\langle M \rangle_n$ is the average force multiplier for $N_H = 10^n$ cm^{-2}. This approximates $\langle M \rangle$ within a factor of ~ 2.

Fig. 6 also shows the dependence of $\langle M \rangle$ on the column density. This is characterized by a decrease followed by an increase with a minimum at $N_H \sim 10^{22}$ cm^{-2}. The minimum is mostly due to the fact that at this column density, the optical depth due to absorption by oxygen is close to unity. For $N_H \leq 10^{22}$ cm^{-2}, the clouds are ionized throughout (Fig. 3) and the decline in $\langle M \rangle$ reflects a decrease in the available X-ray flux. For $N_H > 10^{22}$ cm^{-2}, the ionization structure is such that the leading edge is neutral enough to absorb a large fraction of the far UV radiation. Since the photon flux at those bands is much larger, it results in an increasing $\langle M \rangle$. The changes in $\langle M \rangle$ are more pronounced for low values of U_x because of the SED shape.

The gas density has only a small influence on the cloud structure, and on $\langle M \rangle$, for $n_H(r = 0) < 10^{11}$ cm^{-3} (Fig. 7). For higher densities, the micro-physics changes (see §3.1) and the changes in $\langle M \rangle$ can amount to a factor ~ 2 between $n_H(r = 0) \sim 10^8$ cm^{-3} and $n_H(r = 0) \sim 10^{14}$ cm^{-3}. As shown below, for the $P_{\text{ext}} \propto R^{-2}$, $N_H = $ const. case, this corresponds to a change of $\sim 40\%$ in terminal velocity. Such changes can be critical for marginally accelerating clouds.

The dependence of $\langle M \rangle$ on the FWHM of oxygen lines is shown in Fig. 8 where we consider FWHM< $16,000$ km s^{-1}, similar to BAL flow velocities. We do not show cases with v_{sound} which are roughly equivalent to FWHM~ 70 km s^{-1}. As expected, broader lines produce larger force multipliers (~ 6 times larger for FWHM~ 3000 km s^{-1} compared with thermal case). The effect is more pronounced for small U_x where there are more lines available to absorb the larger continuum flux. For $U_x = 10^{-0.2}$ there is a decrease in $\langle M \rangle$ for FWHM$\gtrsim 3000$ km s^{-1} due to changes in ionization structure which mask the rel-
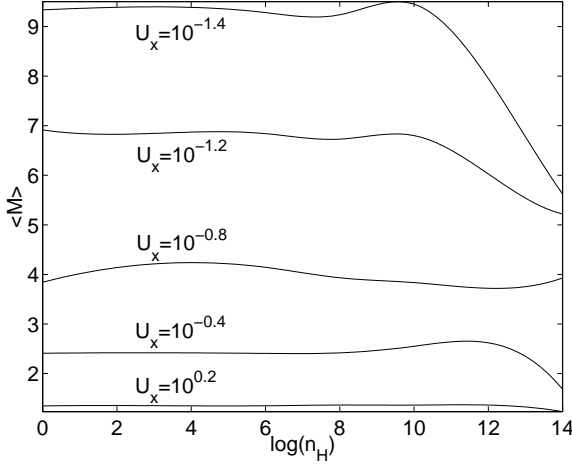
Figure 7. Average force multiplier as a function of $n_H(r = 0)$ for the standard model with v_T and different U_x. For $n_H < 10^{11}$ cm^{-3}, $\langle M \rangle$ is roughly constant. The changes in $\langle M \rangle$ at high densities are due to the changes in the micro-physics of the gas.
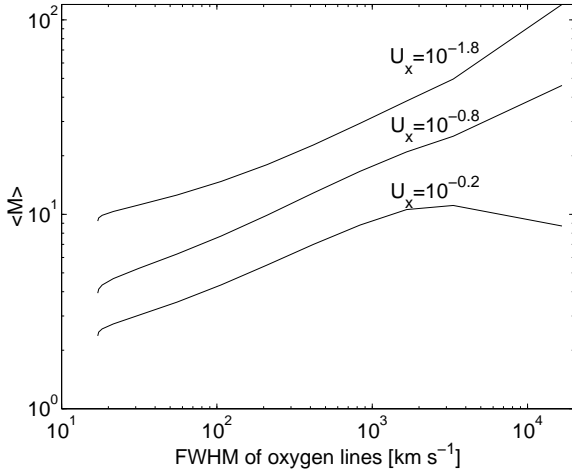

Figure 8. $< M >$ as a function of the FWHM of oxygen lines. Note the logarithmic scales, and the incline of $\langle M \rangle$ (for $U_x < 10^{-0.2}$) towards large FWHM values, which characterise BAL flows.

atively small increase in line contributions. For FWHM$\gtrsim$ 16,000 km s^{-1}, $\langle M \rangle$ is relatively constant since the lines are optically thin relative to the bound-free processes.

While the cloud structure and, therefore, the radiation pressure force are relatively insensitive to the exact shape of the SED (i.e., α_x, α_{ox}) for the same U_x, the exact value of $\langle M \rangle$ depends roughly linearly on the X-ray (0.1-1keV) to total luminosity ratio (equation 4) which in our case is ~ 0.04.

3.3 Approximations for $\langle M \rangle$

Fig. 9a illustrates the most important contributions to $\langle M \rangle$ with respect to the cloud dynamics. While the exact value depends on the cloud's structure, the bound-free force multiplier, M_{bf}, is, in general, a good approximation to $\langle M \rangle$. It is possible to estimate M_{bf} by considering oxygen, the

most abundant metal. Assuming cross sections of the form $\sigma = \sigma_0 (E/E_0)^{-s}$, where E_0 is the ionization energy, σ_0 the edge cross section, $s \simeq 2.5 - 3$, and an X-ray spectrum with an energy power-law index α_x. For an ion X with a number density n_x we find

$$M_{bf} = \frac{1}{\alpha_x + s - 1} \left(\frac{n_X}{n_e} \right) \left(\frac{\sigma_0}{\sigma_T} \right) \left(\frac{L_E(E_0)E_0}{L_{tot}} \right), \qquad (14)$$

where $L_E(E_0)$ is the monochromatic flux at the ionization edge. For the range of interest, $10^{-1.8} \leq U_x \leq 10^{-0.2}$, and the chosen SED, the main contributions to the force multiplier are O VII, O VIII, and He II. Applying the relevant constants, and assuming $X_{O VII} + X_{O VIII} \simeq 1$, we obtain the following estimate:

$$M_{bf} \simeq 1.6 + 1.3 X_{O VIII} + 2 \left(\frac{X_{He II}}{10^{-4}} \right), \qquad (15)$$

where $10^{-6} \lesssim X_{He II} \lesssim 10^{-4}$. This M_{bf} is within a factor ~ 3 of $\langle M \rangle$ for line width given by v_T. This result as well as the general (all elements) M_{bf} is *significantly* different from the force multiplier calculated by Mathews & Veilleux (1989) who considered gas with much lower ionization stages and calculated only the contribution due to the carbon edge. For the typical U_x and SED considered here this gives a value of $\langle M \rangle$ which is a factor of 50(!) smaller than the one calculated by us.

3.4 Cloud dynamics

Solving the equation of motion (equation 12) requires the value of $\langle M(R) \rangle$ for every R. The formal solution, assuming $v(R_0) = 0$, is

$$v(\xi) = v_c \left[\int_1^\xi \left(\langle M(\xi') \rangle - \frac{1}{l} \right) \frac{d\xi'}{\xi'^2} \right]^{1/2}, \qquad (16)$$

where $\xi = R/R_0$. The characteristic velocity v_c is defined as

$$v_c = \sqrt{\frac{1}{1.18 m_H} \frac{\sigma_T L_{tot}}{2\pi c R_0}} \simeq 1350 \left(\frac{L_{45}}{R_{17}} \right)^{1/2} \text{ km s}^{-1}, \qquad (17)$$

where L_{45} and R_{17} are the luminosity in units of 10^{45} erg s^{-1} and the initial distance (R_0) in units of 10^{17} cm. The dynamical problem is thus reduced to the calculation of a single quantity, $\langle M(R) \rangle$, at each position along the cloud trajectory.

We have studied velocity profiles for two generic cases: shell-like clouds with constant mass ($\Omega R^2 N_H = $ const) and constant column density clouds ($N_H(R) = $ const). The exact numerical solutions are shown in Fig. 10. The diagram illustrates the lower velocities that are obtained for the constant column density clouds since these are more massive (note that a comparison between the two is not straight forward since $\langle M \rangle$ is a non-monotonic function of N_H, e.g., §3.3). For the standard model, the velocities are of the same order as the escape velocity at the base of the flow. In particular, velocities of 1000–3000 km s^{-1} are typical of HIG clouds originating in or just outside the BLR. Much larger velocities are achieved for higher density clouds that originate inside the BLR (related, perhaps, to the inner accretion disc). For example, the standard model with $n_H = 10^{12}$ cm^{-3} and constant column density results in a terminal velocity of

$\sim 20{,}000$ km s^{-1} for line width given by $v_{\rm sound}$. Thus, acceleration by X-ray radiation pressure is capable of producing BAL-type flows in AGN. This conclusion applies only to the ballistic motion of hydrostatically stable clouds. Wind-type flows may be different and will be discussed in future works.

Three cases of external pressure powerlaws were examined for constant column density clouds and for constant mass shells, all with $n_H < 10^{11}$ cm^{-3} (see Fig. 10). The main results are explained using the constant column density cloud case.

The first case $U_x(R) = $ const $(\alpha = -2)$. Here $\langle M(R) \rangle$ is a constant of motion and equation (16) results in

$$v(R) = v_{\rm final} \sqrt{1 - \frac{R_0}{R}}. \qquad (18)$$

where the final (asymptotic) velocity is

$$v_{\rm final} = v_c \left[\langle M(U_x) \rangle - \frac{1}{l} \right]^{1/2}. \qquad (19)$$

The final velocity of marginal outflows is therefore very sensitive to the value of l since $1/l \simeq \langle M \rangle$ (Fig. 9b) The acceleration time-scale, defined as the time it takes the cloud to reach 90% of its asymptotic velocity, is

$$t_{\rm accel} \simeq 150 \frac{v_c}{v_{\rm final}} R_{17} \text{ years}. \qquad (20)$$

In the two other cases, U_x decreases with R $(\alpha > -2)$ and U_x increases with R $(\alpha < -2)$ (see Fig. 10). In the first case, the acceleration due to the radiation pressure force decreases as $1/\xi$ to some (positive) power for our range of α. For $\xi \gg 1$, the clouds become asymptotically neutral and the radiation acceleration drops to zero.

In the second case, U_x increases with R, the clouds become more ionized as they move out, bound-bound and bound-free processes become less efficient and at large ξ, the only driving force is due to Compton scattering.

The condition for asymptotic outflow $(\xi \gg 1)$ is that the cloud velocity exceeds the escape velocity at some distance,

$$v(R) > v_{\rm esc}(R) = \sqrt{\frac{1}{1.18 m_H} \frac{\sigma_T L_{\rm tot}}{2\pi c R l}} = v_c \sqrt{\frac{1}{l}}. \qquad (21)$$

Contrary to other wind solutions, in which the final velocity is of the order of $v_{\rm esc}(R_0)$, the final velocity in our model depends on the value of $[M(R)l - 1]$ (equation 16) which can be much larger than unity.

Fig. 10 also shows that a fair fraction of the final velocity is obtained at small ξ. This is the reason for the similar terminal velocity in the $\alpha = -2$ and the $\alpha = -3/2$ cases. A different behaviour is seen for $\alpha = -10/3$ where the gravitational force exceeds the radiation pressure force at $\xi \sim 3$, resulting in a marginal outflow.

The dynamics of constant mass gas shells follows the same trend for the various external pressure profiles, but with higher terminal velocities. This results from the decrease in column density with distance and the fact that for $N_H < 10^{22}$ cm^{-2}, $\langle M \rangle$ is a monotonically decreasing function of N_H (see Fig. 6).

So far we have considered radial motion only. Other AGN components, such as the BLR and the accretion disc, are thought to be rotating around the central mass, and a plausible assumption is to associate a rotational motion to the HIG. Introducing Keplerian velocities (see also §3.5) at
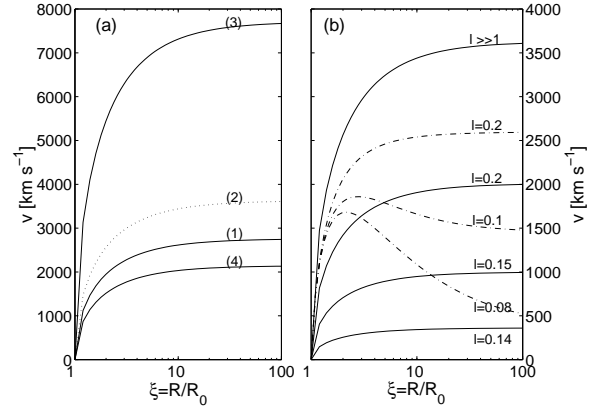

Figure 9. Velocity profiles for $U_x = 10^{-0.8}$, $N_H = 10^{22}$ cm^{-2}, $R_0 = 10^{17}$ cm, L $= 10^{45}$ erg s^{-1}, $l \gg 1$, and $P_{\rm ext} \propto R^{-2}$. Left: $v(\xi)$ for different approximations of $\langle M \rangle$: (1) Exact solution for thermal line width (v_T). (2) like (1) but line width is given by $v_{\rm sound}$, (3) $\langle M \rangle = M(r=0)$, (4) $\langle M \rangle = M_{\rm bf}(r=0)$. As illustrated, the cloud's dynamics is dominated by bound-free absorption for both v_T and $v_{\rm sound}$ line profiles. Right: $v(\xi)$ for different values of l. line width is given by $v_{\rm sound}$. Note the large differences in $v_{\rm final}$ for $1/l \simeq \langle M \rangle$. Solid lines are for clouds with pure radial motion. Dash-dot lines are for clouds with asimuthal (Keplerian) velocities at $\xi = 1$ (see text). Super Eddington luminosities are included for completion.
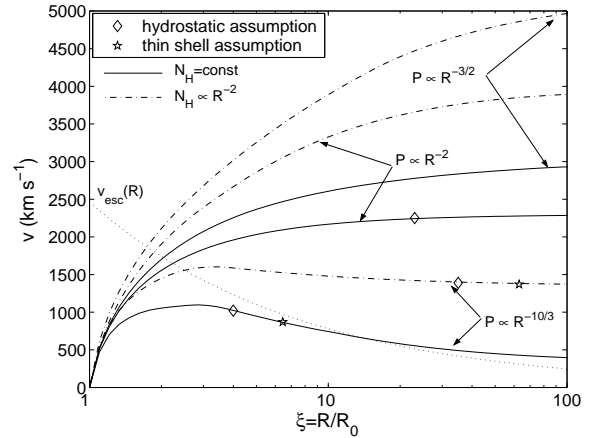

Figure 10. The dependence of $v(\xi)$ on $P_{\rm ext}$ for a case of $U_x = 10^{-0.8}$, $N_H(R_0) = 10^{22}$ cm^{-2}, $R_0 = 10^{17}$ cm, L $= 10^{45}$ erg s^{-1}, $l = 0.3$. Constant N_H cloud profiles in solid lines, and constant mass shell $(N_H \propto R^{-2})$ in dashed line. The escape velocity, $v_{\rm esc}(R)$, is shown for comparison. For $\alpha = -10/3$, gravity takes over due to the rapid expansion of the cloud. Note the critical points beyond which the hydrostatic and the thin shell assumptions are no longer valid (see text).

R_0, while conserving angular momentum along its trajectory, will decrease the effective gravity (in equation 12, the term $1/l$ will be replaced by $1/l(1 - 1/\xi')$) thus increasing the final velocities (see Fig. 9b).

The obtained dynamical results differ significantly from the few previous calculations involving acceleration of clouds by X-ray radiation pressure force. It is an order of magnitude difference from the Mathews & Capriotti (1985) results (see their table 1) and this is not surprising since previous works did not consider the relevant parameter space for the

HIG and, therefore, did not include the relevant radiation absorption mechanisms.

3.5 Limitations and extensions of the model

We have made two critical assumptions: thin shell clouds (which is always true, by construction, at R_0) and hydrostatic equilibrium at all locations. Below we derive general expressions for a critical, normalized distance, ξ_c, beyond which one or both of these assumptions fail.

The critical distance for the thin-shell approximation is

$$\xi_c^{(\text{thin})} = \begin{cases} \left(\frac{R_0}{\Delta R_0}\right)^{\frac{1}{\beta - \alpha - 1}} & \beta - \alpha > 1 \\ \infty & \text{otherwise} \end{cases} \tag{22}$$

where we have used $n_H \propto P_{\text{ext}}$. Here, $\beta = 0, -2$ for constant column density clouds and constant mass shells, respectively. Since the initial conditions are such that $\Delta R_0/R_0 \ll 1$, we see that in general $\xi_c^{(\text{thin})} \gg 1$.

A quasi-hydrostatic cloud structure can be obtained provided the cloud's sound crossing time is shorter than the time it takes the external conditions (i.e., external pressure) to change considerably (e.g., Blumenthal & Mathews 1975) as a result of the cloud's motion. This time is roughly R_0/v_{final}. The quasi-hydrostatic approximation is therefore valid provided $\xi \ll \xi_c^{(\text{hyd})}$ where

$$\xi_c^{(\text{hyd})} \sim \left(\frac{v_{\text{sound}}}{v_{\text{final}}} \frac{R_0}{\Delta R_0}\right)^{\frac{1}{\beta - \alpha}}. \tag{23}$$

In cases where $\beta - \alpha \leq 0$, the cloud structure and dynamics can be treated by our model for all $\xi \geq 1$ provided $R_0 v_{\text{sound}}/(\Delta R_0 v_{\text{final}}) > 1$. In conclusion, cases for which $\xi_c = \min(\xi_c^{(\text{thin})}, \xi_c^{(\text{hyd})}) < 1$ cannot be treated by our model.

Considering specific examples, we note that for the standard model, with $L_{45} = 1$, $R_{17} = 1$, $l = 0.3$, $U_x(R_0) = 10^{-0.8}$, and $\alpha = -2$, numerical calculations give $\xi_c \simeq 20$. At $\xi = 4$ the cloud is already moving at 90% of its final velocity. For two other cases of $\alpha = -2$ ($N_H \propto R^{-2}$) and $\alpha = -1.5$, the approximations hold throughout the region. The case of $\alpha = -10/3$ is different due to the rapid expansion of the cloud. In this case, for $N_H = \text{const}$, our model approximations break at small ξ ($\xi_c \simeq 4$).

Throughout this paper we assumed an external pressure that depends only on R. This is a natural assumption for the constant mass (thin spherical shell) case. For the other case, where the column density decrease with distance is slower than $N_H \propto R^{-2}$, we can imagine a situation where the cloud subtends a small solid angle ($\Omega < 4\pi$) and the external pressure profile is angle dependent. Clouds with finite lateral extents are prone to evaporation through their rims due to pressure gradients inside the cloud (e.g., Mathews & Veilleux 1989, equation 1). This sets a lower limit on the cloud's lateral extents and conversely on the spatial angle it subtends of

$$\frac{\Omega}{4\pi} \gtrsim 10^{-2} \left(\frac{v_{\text{sound}}}{v_{\text{final}}}\right)^2. \tag{24}$$

Filamentary structure, and different dynamics in different directions, can be introduced into our formalism. The treatment of the general two dimensional problem is beyond the scope of this paper (for simple pancake shaped clouds see Blumenthal & Mathews 1979).

In this work we have considered general confinement, having in mind external magnetic pressure. Confinement by hot thermal gas is another possibility that has been discussed, extensively, in the literature. The presence of highly ionized, dilute gas between the clouds cannot be ruled out. Relative velocities between such gas and the cloud will result in drag forces that tend to decrease the final velocities. The cloud-gas boundary may be subjected to various instabilities which may affect the cloud structure considerably and ultimatly lead to its destruction. This complex situation cannot be solved using the methods adopted here.

4 CONCLUSIONS

We have made detailed numerical calculations of the dynamics of highly ionized gas clouds that are in pressure equilibrium with external magnetic pressure and are ionized by a typical AGN continuum. The self-consistent calculations include the ionization and thermal equilibrium of the cloud, the radiative transfer and the one-dimensional hydrostatical equilibrium solution. The principal conclusion is that such highly ionized clouds can be accelerated to high velocities by means of radiation pressure acceleration. The dynamical problem can be reduced to the calculation of a single parameter, the average force multiplier, $\langle M \rangle$. The terminal velocity of the flow scales like the escape velocity at its origin but can exceed this velocity by a large factor ($\sim \sqrt{\langle M \rangle}$). The cloud velocity is sensitive to the confining pressure profile (α), especially for marginal flows. In particular, flows that originate just outside the BLR in objects with $L_{\text{tot}} \simeq 10^{45}$ erg s^{-1}, will reach velocities of $1000 - 3000$ km s^{-1}, similar to the velocities measured for the X-ray and UV absorption lines. Highly ionized AGN clouds are driven mainly by bound-free absorption and bound-bound processes are less important unless significant non-thermal line broadening or very low column densities ($< 10^{20}$ cm^{-2}) are involved.

REFERENCES

Arav N., Li Z., Begelman M. C., 1994, ApJ, 432, 62
Begelman M., de Kool M., Sikora M., 1991, ApJ, 382, 416
Blumenthal G. R., Mathews W. G., 1975, ApJ, 198, 517
Blumenthal G. R., Mathews W. G., 1979, ApJ, 233, 479
Bottorff M. C., Korista K. T., Shlosman I., 2000, ApJ, 537, 134
Bottorff M.C., Ferland G.J., 2000, MNRAS, 316, 103
Castor J., Abbott D., Klein R., 1975, ApJ, 195, 157
Contini M., Viegas S. M., 1999, ApJ, 523, 114
Crenshaw D. M., Kraemer S. B., Bogess A., Maran S. P., Mushotzky R. F., Wu C., 1999, ApJ, 516, 750
Crenshaw D. M., Kraemer S. B., 1999, ApJ, 521, 572
de Kool M., Begelman M. C., 1995, ApJ, 455, 448
Elitzur M., Ferland G., 1986, ApJ, 305, 35
George I. M., Turner T. J., Netzer H., Nandra K., Mushotzky R., Yaqoob, T., 1998, ApJS, 114, 73
George I. M., Turner T. J., Yaqoob T., Netzer H., Laor A., Mushotzky R. F., Nandra K., Takahashi T., 2000, ApJ, 531, 52

Guainazzi M., Mihara T., Otani C., Matsuoka M., 1996, PASJ, 48, 781

Hamann F., Netzer H., & Shields J. C., 2000, ApJ, 536, 101

Kaiser et al., 2000, ApJ, 528, 260

Kaastra J. S., Mewe R., Liedhal D. A., Komossa S., Brinkman A. C., 2000, A&A, 354, L83

Kaspi S., Brandt W. N., Netzer H., Sambruna R., Chartas G., Garmire G. P., Nousek J. A., 2000, ApJ, 535, L17

Kaspi S., Brandt W. N., Netzer H., George I. M. , Chartas G., Behar E., Sambruna R., Garmire G. P., Nousek J. A., 2001, ApJ, submitted

Komossa S., Meerschweinchen J., 2000, A&A, 354, 411

Kraemer S. B., Ruiz J. R., Crenshaw D. M., 1998, ApJ, 508, 232

Krolik J. H., 1979, ApJ, 228, 13

Krolik J. H., McKee C. F., Tarter C. B., 1981, ApJ, 249, 422

Krolik J. H., Kriss G. A., 1995, ApJ, 447, 512

Mathews W. G., 1975, ApJ, 198,517

Mathews W. G., Blumenthal G.R., 1977, ApJ, 214, 10

Mathews W. G., Capriotti E. R., 1985, in Miller, J. S., ed., Astrophysics of Active Galaxies and Quasi-Stellar Objects. University Science Books, p. 185

Mathews W. G., 1986, ApJ, 305, 187

Mathews W. G., Ferland G. J., 1987, ApJ, 323, 456

Mathews W. G., Veilluex S., 1989, ApJ, 336, 93

Mathews W. G., 1992, ApJ, 386, 90

Mathur S., Wilkes B., Elvis M., Fiore F., 1994, ApJ, 434, 493

Mathur S., Elvis M., Wilkes B., 1995, ApJ, 452, 230

Mihalas D., Mihalas B., 1999, Foundations of Radiation Hydrodynamics. Dover publications, NY

Murray N., Chiang J., Grossman S. A., Voit G. M., 1995, ApJ, 451, 498

Murray N., Chiang J., 1995, ApJ, 454, L105

Netzer H., 1990, in Courvoisier T.J.-L.& Mayor M., eds., Active Galactivc Nuclei. eds., Springer-Verlag, Berlin, p. 57

Netzer H., 1996, ApJ, 473, 781

Netzer H., Turner T. J., George I. M., 1998, ApJ, 504, 680

Otani C., et al., 1996, PASJ, 48, 211

Proga D., Stone J. M., & Kallman T. R., 2000, ApJ, 543, 686

Rees M. J., 1987, MNRAS, 228, 47

Reynolds C. S., Fabian A. C., 1995, MNRAS, 273, 1167

Reynolds C. S., 1997, MNRAS, 286, 513

Sambruna R. M., Netzer H., Kaspi S., Brandt W. N., Chartas G., Garmire G. P., Nousek J. A., Weaver K. A., 2000, ApJ, in press (astro-ph/00010356)

Sivron R., Tsuruta S., 1993, ApJ, 402, 420

Srianand R., 2000, ApJ, 528, 617

Turner T. J., George I. M., Nandra K., Mushotzky R. F., 1997, ApJS, 113, 23

Weymann R., 1976, ApJ, 208, 286